Batteries & Supercaps

Research Article
doi.org/10.1002/batt.202300447

Chemistry Europe
European Chemical Societies Publishing

www.batteries-supercaps.org

Nanoengineering of Thin Film V_2O_5 Cathode Interfaces via Atomic Layer Deposition for use with Polymer Gel Ionic Liquid Electrolytes

Aaron O'Donoghue,[a] Micheál Shine,[a] Ian M. Povey,[a] and James F. Rohan*[a]

In this work we show high capacity and cycle-life performance, for electrodeposited, crystalline V_2O_5 thin film cathodes protected by a 1 nm ALD alumina deposit for use with Li-metal and ionic liquid electrolyte based microbatteries. Al_2O_3 coatings thicker than 1 nm are shown to decrease the performance of the V_2O_5 thin film cathodes. The ionic liquid outperforms an organic electrolyte at 1 C rates with an initial capacity of 148 mAh g^{-1} and capacity retention of 97% at cycle 50. A polymer gel analogue of the ionic liquid electrolyte in combination with the 1 nm Al_2O_3 coated V_2O_5 had an initial capacity of 139 mAh/g with a capacity retention of 93.5% to cycle 800, illustrating high capacity and extended cycle life.

Introduction

Vanadium pentoxide (V_2O_5) is a promising high energy density cathode for lithium-based batteries.[1] V_2O_5 suffers from poor charge-discharge kinetics due to its low ionic diffusion and electronic conductivity.[2,3] Coatings such as ITO,[4] TiO_2[5] and Al_2O_3[6] have previously been reported to improve the charge-discharge kinetics of V_2O_5 in typical organic electrolytes. Similarly, coatings such as Al_2O_3,[7–9] MgO[10] and TiO_2[11] have previously been reported to improve charge-discharge kinetics on other oxide-based cathode materials such as $LiCoO_2$.

Al_2O_3 coating via atomic layer deposition (ALD) has been reported previously by Liu et al. using a V_2O_5 xerogel.[6] A sol-gel method gave an electrode thickness ~2 μm. They cycled the electrode over a 2 V range indicating that the 2 e$^-$ Li potential window was used and achieved a maximum capacity of 225 mAh g^{-1} with 10 ALD cycles (approximately 1 nm Al_2O_3) coated V_2O_5. Data was only provided for the first 50 cycles and it has been reported by Ng et al. that potential ranges for 2 and 3 e$^-$ V_2O_5 reactions can exhibit poor capacity retention by comparison with the 1 e$^-$ potential window of 2.5 to 4 V.[12]

Microbatteries are designed primarily for use in micro-devices such as medical devices, or IoT (internet of things) sensors where solid-state electrolytes such as LiPON can be utilised rather than the standard volatile organic electrolytes which are less easily fabricated at the microdimensions.[13] Solid-state electrolytes are also limited by their low ionic conductivities of 3×10^{-3} mS cm^{-1}, hindering high-rate capability which may be required to counter their small size during periods of data acquisition or communication.[14] McGrath and Rohan reported the use of ionic liquids with V_2O_5 which have low volatility and comparable conductivities to organic electrolytes.[15] A polymer-gel ionic liquid (PGIL) electrolyte was also reported which acts as a quasi-solid-state electrolyte with an ionic conductivity 1.9 mS cm^{-1} which is over two orders of magnitude greater than typical solid-state electrolyte and closer to typical organic electrolytes (e.g. 7.9 mS cm^{-1} for 1 M $LiPF_6$ in (1 : 1) EC : DEC).[16,17]

In this work, we initially investigate increasing deposition times of V_2O_5 to increase the layer thickness and capacity while also reducing the total ratio of inactive material in the cell.[18] This was followed by an investigation of the performance of V_2O_5 thin films (~200 nm) on which Al_2O_3 coatings deposited via ALD were utilised to protect the cathode from unwanted electrolyte interactions and increase cycle life. The results for ALD coated cathodes in organic, ionic liquid and PGIL electrolytes are compared.

Results and Discussion

V_2O_5 thin films were deposited and annealed to a crystalline morphology on a hotplate at 325 °C in ambient air, as described previously, where a 10 s deposition time yielded a thickness of 220 nm.[15,19]

Figure 1 shows Raman spectra for 10, 40 and 90 s deposition time V_2O_5. The spectra align closely with the previously reported data for the orthorhombic phase of V_2O_5.[20–23] That phase of V_2O_5 is characterized by a well-established spectrum and belongs to the space group Pmmn with D2 h point symmetry.[24,25] The peaks observed in the annealed films correspond to various vibrations including: In-phase stretching of V=O1 bonds at 994.51 cm^{-1}, Anti-phase stretching of V–O2 bonds at 705.40 cm^{-1}, The x-axis displacement of stretching O2 atoms at 528.4 cm^{-1}, The bending of the V–O3-V bridge angle at 484.81 cm^{-1}, The x-axis displacement of O1 atoms at

[a] A. O'Donoghue, M. Shine, Dr. I. M. Povey, Dr. J. F. Rohan
Tyndall National Institute, Lee Maltings, University College Cork, T12 R5CP Cork, Ireland
E-mail: james.rohan@tyndall.ie

Supporting information for this article is available on the WWW under https://doi.org/10.1002/batt.202300447

Research Article
doi.org/10.1002/batt.202300447
Chemistry Europe
European Chemical Societies Publishing

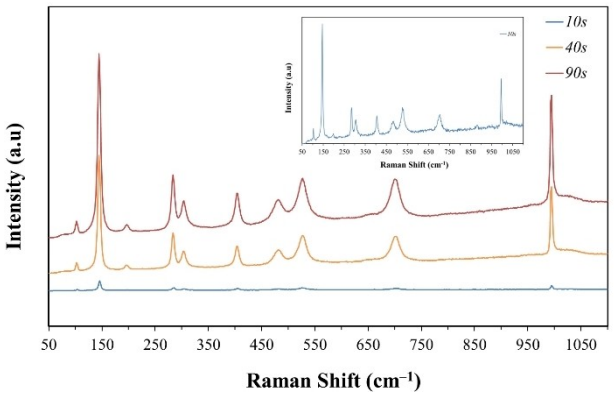

Figure 1. Raman profile of 10 (Intensity expanded in the inset), 20 and 90 s deposition time V_2O_5.

403.79 cm^{-1}, The z-axis displacements of $O2_1$ and $O2_2$ atoms at 302.36 cm^{-1}, The y-axis displacement of O1 atoms at 284.43 cm^{-1}, The x-axis displacement of V atoms at 200.12 cm^{-1}, The O3–V–O2 in the y-axis at 144.73 cm^{-1}, and the vibration of V atoms within the O3–V–O2 bridge along the z-axis at 101.35 cm^{-1}.

The peaks at 200.12 cm^{-1} and 144.73 cm^{-1} correspond to lattice vibrations and are strongly indicative of the layered structure.[26–28] The lower intensity 10 s spectra was expanded in the inset in figure 1 to show peak positions. It can be seen that the spectra for all samples share the same peak positions however, intensity increases proportionally with deposition time or thickness when the experimental conditions are adequately controlled.[29]

V_2O_5 thin film deposits were cycled in an ionic liquid electrolyte 0.5 M LiTFSI in [C_4mpyr][TFSI] using cyclic voltammetry (CV) at 0.05 mV s^{-1} as shown in figure 2. At short deposition times variation in thickness measured on a profilometer was small. At longer deposition times the variation increased, and very little additional capacity could be achieved beyond the 90 s deposition (Supporting information, S1 and S2). The surface resistance increases during deposition leading to preferential and uneven plating at the substrate edge for these resistive oxides.[30,31]

Sharp peaks are observed in the CVs for 10 and 20 s deposition times which show 2 pairs of anodic and cathodic peaks typical of V_2O_5 within the 2.5–4 V region with peaks corresponding to α↔ε and ε↔δ phases which occur during intercalation/deintercalation.[32–34] It can be seen that with each increase in deposition time from 10 s that peak current increases along with the anodic and cathodic peaks shifting to higher overpotential, due to the increase in Li^+ diffusion pathways and cathode resistance.[35,36,37]

The maximum capacities for each sample were 10, 15, 25, and 32 μAh for 10, 20, 40 and 90 s, respectively.[38] To investigate if the samples could be more completely crystallised yielding larger capacities, oven annealing at 450 °C for 7 hours in ambient air was employed on 10, 40 and 90 s deposited samples. The upper potential limit for 90 s was increased from 3.65 to 3.8 V still within the maximum range of 2.5–4 V recommended for the 1 e^- reaction without decreasing the cycling stability. A third anodic peak was also observed at 3.25 V for the thickest 90s deposit when oven annealed which has been reported previously[39–41] and probably result from slight changes in the phase orientation for the thicker deposits.

The capacities of hotplate and oven annealed samples were compared. The thinner deposits did not show a significant change in capacity dependent upon the annealing conditions. However, for the 40 s oven annealing an 84% increase in capacity from 24 to 48 μAh was observed while the 90 s deposit showed a 156% increase in capacity 32 to 82 μAh (or 144 mAh g^{-1} assuming a 1.7 μm deposit). Figure 3 shows capacities and coulombic efficiencies for a 90 s deposited sample to 100 cycles using CV. An Initial capacity of 51 μAh was observed. After 25 cycles, a maximum capacity of 82 μAh is achieved before decreasing to 69 μAh at 100 cycles for a capacity retention of 84%.

CV analysis was utilized to determine the effect of coating the V_2O_5 with 1, 2 and 3 nm Al_2O_3 deposited by ALD. Figure 4 shows CV plots for the three coatings used in 0.5 M LiTFSI in [C_4mpyr][TFSI] and 1 M $LiPF_6$ in EC:DEC (1:1). Figure 4 (a) shows the 30th cycle at 0.1 mV s^{-1} in ionic liquid electrolyte. The electrode with a 1 nm coating shows sharp peak formation with the same peak position as the uncoated sample. The 2 nm

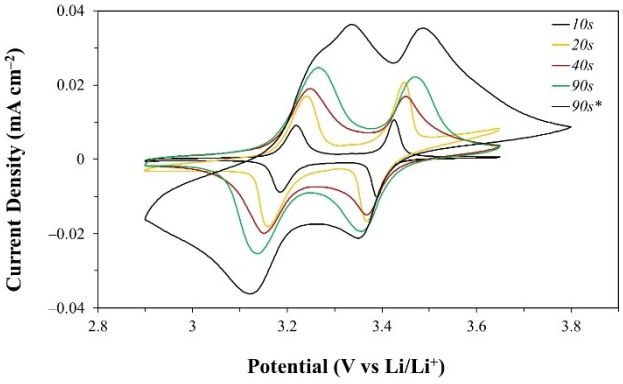

Figure 2. CV profiles of cycle 5 for 10–90 s deposition time V_2O_5 in ionic liquid electrolyte at 0.05 mV s^{-1}; vs. Li/Li^+. (* = oven annealed).

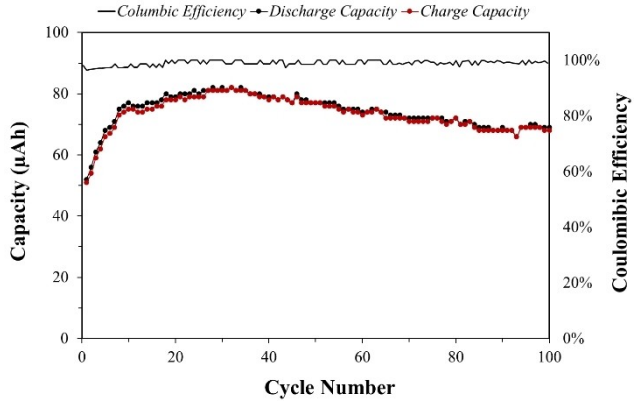

Figure 3. Capacity and coulombic efficiency of 90 s deposition time oven annealed V_2O_5 in ionic liquid electrolyte at 0.05 mV s^{-1}; vs. Li metal.

Research Article
doi.org/10.1002/batt.202300447
Chemistry Europe
European Chemical Societies Publishing

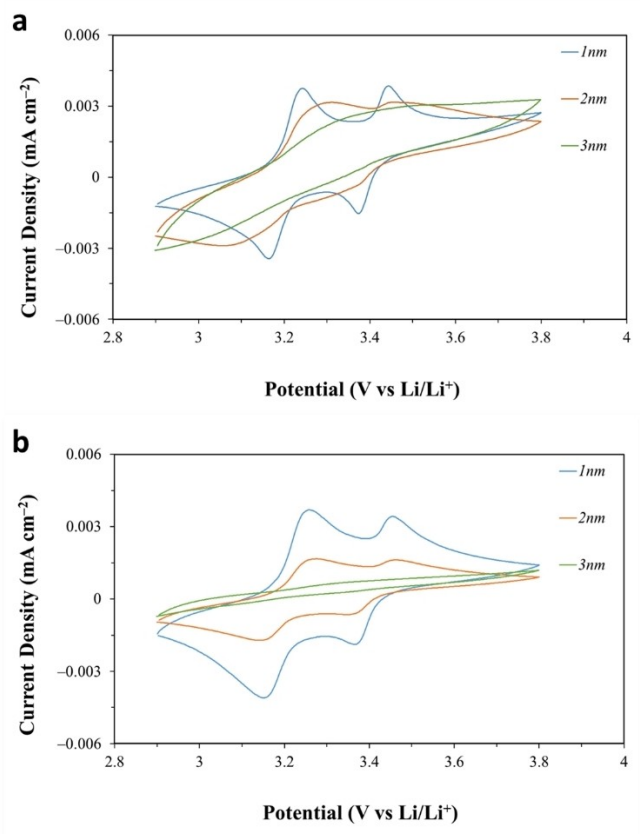

Figure 4. Cycle 30 for 1–3 nm Al_2O_3 coated V_2O_5 (10s deposit) in (a) ionic liquid and (b) organic electrolyte at 0.1 mV s^{-1}; vs. Li metal.

coating shows inhibited peak formation for the V_2O_5, with the cathodic peak at 3.08 V shifted partially outside the lower potential limit. This indicates an increase in overpotential or charge transfer resistance inlch the thicker 2 nm Al_2O_3 acts as an electrochemically resistive layer.[42] This is further exacerbated for the 3 nm which shows little or no lithium in V_2O_5 peak behaviour. Figure 4 (b) is the 30th cycle at 0.1 mV s^{-1} in organic electrolyte. A similar trend is observed to the ionic liquid with the 1 nm Al_2O_3 coating showing sharp peak formation. The 2 nm Al_2O_3 coating leads to a decreased peak current height. Again, the 3 nm coating is too resistive and no V_2O_5 peaks are resolved at this sweep rate. The CV profiles indicate that increasing coating thickness over 1 nm has a significantly negative effect on the charge-discharge kinetics.[43]

Figure 5 shows discharge capacities obtained from galvanostatic cycling (GC) at 1 C using an organic electrolyte for bare V_2O_5 and 1 nm Al_2O_3 coated V_2O_5 and a 1 nm coated V_2O_5 with an ionic liquid electrolyte. Bare V_2O_5 with organic electrolyte had an initial capacity of 135 mAh g^{-1} and a capacity retention of 60% at cycle 50. 1 nm Al_2O_3 coated V_2O_5 when cycled in organic electrolyte had an initial capacity of 145 mAh g^{-1} and a capacity retention of 80% at cycle 50. For the ionic liquid option, the 1 nm Al_2O_3 coated V_2O_5 had an initial capacity of 148 mAh g^{-1} and a capacity retention of 97% at cycle 50. These results show that 1 nm Al_2O_3 coating significantly improves the performance over bare V_2O_5 for both organic and ionic liquid

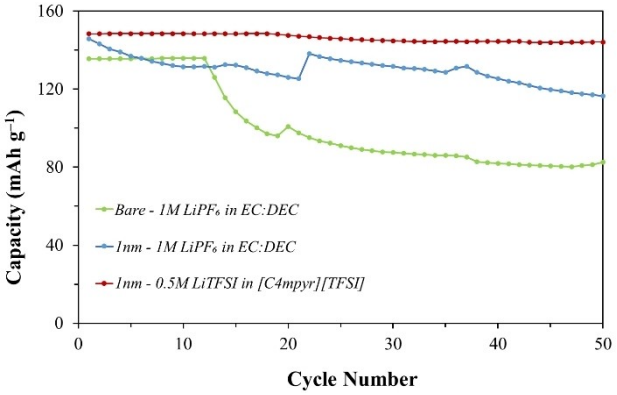

Figure 5. Comparative discharge capacities of bare and 1 nm Al_2O_3 coated V_2O_5 (10s deposit) in organic electrolyte and 1 nm Al_2O_3 coated V_2O_5 in ionic liquid electrolyte at 1 C vs. Li metal.

electrolytes and that the ionic liquid shows much greater capacity retention at cycle 50. Ionic liquids based on both pyrrolidinium and $TFSI^-$ have shown improved cyclability due to more stable SEI formation containing F and N element species which can improve Li-ion diffusio–[44–46] We have previously reported[15] that discharge capacities for the same ionic liquid without and with a vinylene carbonate additive at 1 C (cycle 30 and 40) were ~90 and ~120 mAh g^{-1}, respectively. In this work 1 nm Al_2O_3 coated V_2O_5 shows capacities of 144 mAh g^{-1} at cycle 40 which is an improvement over the previous analysis for ionic liquids with and without the carbonate additive.

Figure 6 shows a comparison of this work and other studies related to V_2O_5 thin film performance at similar cycle-life and C rate.[47,48] Previous reported results from this laboratory with a 3% wt. % vinylene carbonate (VC) electrolyte additive showed a capacity of ~120 mAh g^{-1} at cycle 30. A capacity of ~85 mAh g^{-1} is observed in this work at cycle 30 for bare V_2O_5 in organic electrolyte. A capacity of ~128 mAh g^{-1} is achieved at cycle 30 for 1 nm coated V_2O_5 in organic electrolyte which is a 7% increase over the performance with VC additive. In organic electrolyte a capacity of ~144 mAh g^{-1} is observed at cycle 30

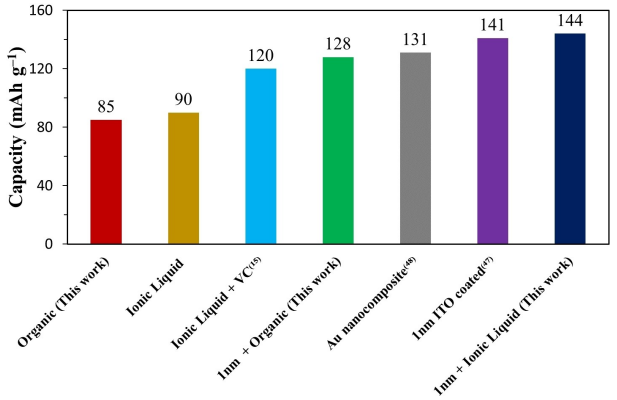

Figure 6. Comparative discharge capacities for this work compared to literature values at similar cycles and C rates.

Research Article
doi.org/10.1002/batt.202300447
Chemistry Europe
European Chemical Societies Publishing

for 1 nm Al_2O_3 coated V_2O_5 which is a 20% increase over the literature optimisation with a VC additive.

Figure 7 shows GC of 1 nm Al_2O_3 coated V_2O_5 in ionic liquid electrolyte, for which the lower potential limit was decreased to 2.6 from 2.9 V for long term cycling to ensure full lithiation and de-lithiation within the potential range. An initial capacity of 150 mAh g^{-1}, was achieved which was stable for ~25 cycles followed by a gradual decrease in capacity. The capacities at cycle 50, 100, 250 and 500 were 132, 119, 112 and 105 mAh g^{-1}, respectively, for a capacity retention 70% at cycle 500.

A PGIL electrolyte was fabricated as described previously.[16] To achieve thinner electrolytes a smaller quantity of the electrolyte was utilised which resulted in a thickness of 95 μm by comparison with 450 μm of the previous work and more in line with typical battery electrolyte thickness.[49] EIS was used at room temperature to determine the ionic conductivity shown in table 1 and compared to LiPON a common commercial solid-state electrolyte, PG-60 from our previous work and 1 M $LiPF_6$ in (1:1) EC:DEC a common organic electrolyte.[14,17] The PGIL had a conductivity ~470 times that of LiPON and the same order of magnitude as both the previous PGIL reported and the common organic electrolyte.

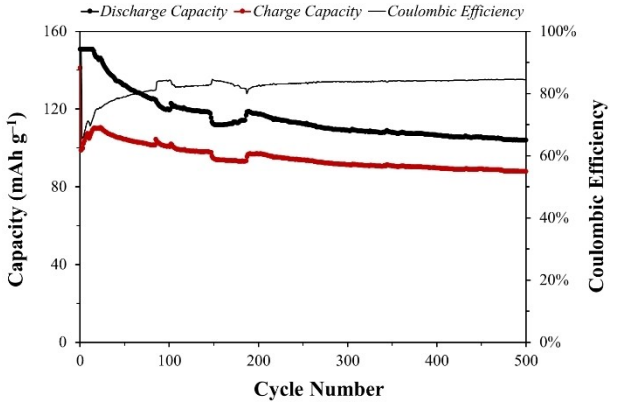

Figure 7. GC of 1 nm Al_2O_3 coated V_2O_5 (10s deposit) in ionic liquid at 1 C vs. Li metal.

Table 1. Comparison of ionic conductivities of polymer gel, solid-state and organic electrolytes.

	LiPON	PG-60	1 M $LiPF_6$ in (1:1) EC:DEC	PGIL
Conductivity (mS cm^{-1})	3×10^{-3}	1.9	7.9	1.43

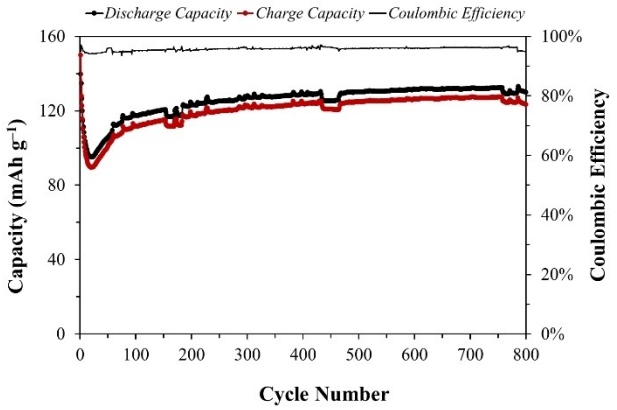

Figure 8. GC of 1 nm Al_2O_3 coated V_2O_5 (10s deposit) with PGIL electrolyte at 1 C vs. Li metal.

Figure 8 shows GC of 1 nm Al_2O_3 coated V_2O_5 with PGIL electrolyte at 1 C. An initial discharge capacity of 139 mAh/g was followed by a decrease in capacity to 95 mAh g^{-1} at cycle 20 before increasing again gradually to 117 mAh g^{-1}, at cycle 100. The initial high capacity followed by a decrease may have been due to poor initial cathode contact between the alumina coated cathode and the PGIL leading to poor intercalation and deintercalation, wtabilizedlised after cycle 25.

Capacities at cycle 500 and 800 were both 130 mAh g^{-1} which is an 8% increase of the previous work at 1 C and demonstrates long term stable cycling with a capacity retention of 93.5% against a lithium metal anode. This is an increase ~10% over the analogous ionic liquid electrolyte, which was also seen in the previous work with a VC additive or PG-60 where the PGIL shower better long-term cycling. This can be further attributed to the SEI formation when a PVDF polymer is utilised. It has been reported that both the LiTFSI salt and the ionic liquid in combination with PVDF and other polymers lead to the formation of a homogenous LiF-rich SEI layer which can allow for uniform Li^+ reaction pathways improving the charge-discharge kinetics and Li plating at the anode. Furthermore, polymer based electrolytes form a thin homogenous SEI unlike for organic liquid electrolytes where their SEI continues to grow during cycling leading to capacity los–[50–52]

Conclusions

Initial CV analysis showed that oven annealing is required for thicker plated V_2O_5 cathodes to obtain high capacity electrochemically active crystalline thin films. The 90 s plated V_2O_5 which was oven annealed showed a maximum capacity of 82 μAh. with a capacity retention of 84% at cycle 100.

Interfacial coatings using ALD were investigated to enhance the stability of the V_2O_5 in longer term cycling. Films thicker than 1 nm were determined to be too resistive and not compatible with the cathode material. 1 nm Al_2O_3 coated V_2O_5 did show improved performance with an initial capacity of 148 mAh g^{-1} exceeding that of the organic electrolyte and had a greater capacity retention of 97% at cycle 50.

A thin 95 μm PGIL electrolyte showed comparable conductivities to 1 M $LiPF_6$ in EC:DEC and previous research with this ionic liquid and polymer gel analogues. In combination with the 1 nm Al_2O_3 coating to protect the interface this PGIL/V_2O_5 combination delivered an initial capacity of 139 mAh g^{-1} and a capacity of 130 mAh g^{-1} at cycle 800 against a lithium metal anode for a capacity retention of 93.5%.

Materials & Methods

V_2O_5 was deposited on Si wafer coupons for which the surface area of the active material was ~0.9 cm^2 (mass loading = 6.05×10^{-5} g) with Ti (10 nm) and Au (200 nm) adhesion and contact layers. The plating bath previously reported included 0.25 M $VOSO_4.xH_2O$ (Sigma Aldrich) dissolved in 1:1 ethanol:dionized water.[53] V_2O_5 was deposited at 2 V using a CH Instruments 660B potentiostat. with a three-electrode cell consisting of a standard calomel reference and platinised Ti mesh counter electrode. The deposited films were annealed using a hotplate and oven annealing method described in the results section.

The thin PGIL was fabricated using $^1/_4$ of the reagents reported previously.[16] Once the PGIL was set it was measured using a micrometre to a thickness of 95 μm and EIS was carried out using a Biologics VSP potentiostat.

Al_2O_3 was deposited to 1, 2 or 3 nm via ALD using a Picosun R200 system at 150 °C. Pulse durations were 0.1 s for both trimethylaluminium (TMA) and water reagents with purge times of 4 and 6 s, respectively. Alumina thin-film growth rate was assumed to be ~0.1 nm per cycl–[54–58] Previous work has shown that for lower than 10 cycles or ~1 nm thickness that island growth during initial nucleation steps can lead to incomplete coverage, a complete monolayer is formed on subsequent cycles where the islands coalesce .[59,60]

Electrochemical performance was determined using a Biologics VSP potentiostat with CV and GC. A pouch cell was fabricated using 0.25 mm Li foil (Sigma Aldrich) as a counter and reference electrodes. Two liquid electrolytes were used, a battery grade organic electrolyte solution of 1 M $LiPF_6$ in EC:DEC (1:1) (Sigma Aldrich) and 0.5 M LiTFSI (Sigma Aldrich) in [C_4mpyr][TFSI] (Solvionic). The cells were assembled and tested in an MBraun LABstar glovebox.

Capacities were calculated from CV by integrating the area under the curve for charge and discharge where current (A) x time (s) = Coulomb (C), Capacities calculated from GC were calculated based on the total time took to reach the upper or lower potential limit so that, s x A = C which can be converted to Ah. mAh/g was obtained by dividing the capacity (mAh) by the cathode mass (g), where mass (g) = density (g/cm^3) x volume (cm^3) based on the surface profiler derived thickness and area of the deposit.

Acknowledgements

This publication emanated from research supported in part by a research grant from Science Foundation Ireland (SFI) and is co-funded by the European Regional Development Fund under Grant Number 13/RC/2077_P2 and the EU Enables Research Infrastructure Project Powering the Internet of Things, funded by the Horizon 2020 programme under grant agreement number 730957. Open Access funding provided by IReL.

Conflict of Interests

The authors declare no conflict of interest.

Data Availability Statement

The data that support the findings of this study are available from the corresponding author upon reasonable request.

Keywords: Alumina · Vanadium Pentoxide · Microbattery · Polymer Gel · Ionic Liquid

[1] Y. Yue, H. Liang, Y. Yue, H. Liang, *Adv. Energy Mater.* **2017**, *7*, 1602545.
[2] X. Chen, E. Pomerantseva, P. Banerjee, K. Gregorczyk, R. Ghodssi, G. Rubloff, *Chem. Mater.* **2012**, *24*, 12.
[3] E. Østreng, K. B. Gandrud, Y. Hu, O. Nilsen, H. Fjellvåg, *J. Mater. Chem. A* **2014**, *2*, –044–15051.
[4] B. Zhao, M. Nisula, A. Dhara, L. Henderick, F. Mattelaer, J. Dendooven, C. Detavernier, B. Zhao, M. Nisula, A. Dhara, L. Henderick, F. Mattelaer, J. Dendooven, C. Detavernier, *Adv. Mater. Interfaces* **2020**, *7*, 2001022.
[5] S. Tian, A. Xing, H. Tang, Z. Bao, G. Wu, *J. Mater. Chem. A* **2014**, *2*,–896–2900.
[6] D. Liu, Y. Liu, S. L. Candelaria, G. Cao, J. Liu, Y.-H. Jeong, *J. Vac. Sci. Technol. A: Vacuum, Surfaces, and Films* **2012**, *30*, 01A123.
[7] T. Teranishi, Y. Yoshikawa, M. Yoneda, A. Kishimoto, J. Halpin, S. O'Brien, M. Modreanu, I. M. Povey, *ACS Appl. Energ. Mater.* **2018**, *1*,–277–3282.
[8] B. Xiao, Q. Tang, X. Dai, F. Wu, H. Chen, J. Li, Y. Mai, Y. Gu, *ACS Omega* **2022**, *7*, –597–31606.
[9] A. O'Donoghue, M. Shine, I. M. Povey, J. F. Rohan, *Int. J. Mol. Sci.* **2023**, *24*, 11207.
[10] Z. Wang, X. Huang, L. Chen, *J. Electrochem. Soc.* **2003**, *150*,–199–A208, DOI: 10.1149/1.1532326/XML.
[11] S. H. Moon, M. C. Kim, E. S. Kim, Y. K. Shin, J. E. Lee, S. Choi, K. W. Park, *RSC Adv.* **2019**, *9*,–903–7907.
[12] S.-H. Ng, T. J. Patey, R. Büchel, F. Krumeich, J.-Z. Wang, H.-K. Liu, S. E. Pratsinis, P. Novák, *Phys. Chem. Chem. Phys.* **2009**, *11*,–748–3755.
[13] D. R. MacFarlane, N. Tachikawa, M. Forsyth, J. M. Pringle, P. C. Howlett, G. D. Elliott, J. H. Davis, M. Watanabe, P. Simon, C. A. Angell, *Energy Environ. Sci.* **2014**, *7*–232–250.
[14] J. F. M. Oudenhoven, L. Baggetto, P. H. L. Notten, *Adv. Energy Mater.* **2011**, – 10–33.
[15] L. M. McGrath, J. F. Rohan, *Batteries & Supercaps* **2021**, *4*–485–492.
[16] L. M. McGrath, J. Jones, E. Carey, J. F. Rohan, *ChemistryOpen* **2019**, *8*,–429–1436.
[17] K. Hayashi, Y. Nemoto, S. I. Tobishima, J. I. Yamaki, *Electrochim. Acta* **1999**, *44*,–337–2344.
[18] J. Wu, X. Zhang, Z. Ju, L. Wang, Z. Hui, K. Mayilvahanan, K. J. Takeuchi, A. C. Marschilok, A. C. West, E. S. Takeuchi, G. Yu, *Adv. Mater.* **2021**, *33*, 2101275.
[19] Y.-R. Lu, T.-Z. Wu, C.-L. Chen, D.-H. Wei, J.-L. Chen, W.-C. Chou, C.-L. Dong, *Nanoscale Res. Lett.* **2015**, *10*, 387.
[20] E. Armstrong, M. O'Sullivan, J. O'Connell, J. D. Holmes, C. O'Dwyer, *J. Electrochem. Soc.* **2015**, *162*,–605–D612.
[21] S. Liu, Z. Tong, J. Zhao, X. Liu, J. Wang, X. Ma, C. Chi, Y. Yang, X. Liu, Y. Li, *Phys. Chem. Chem. Phys.* **2016**, *18*, –645–25654.
[22] C. Sanchez, J. Livage, G. Lucazeau, *J. Raman Spectrosc.* **1982**, *1*– 68–72.
[23] P. Shvets, O. Dikaya, K. Maksimova, A. Goikhman, *J. Raman Spectrosc.* **2019**, *50*,–226–1244.
[24] R. Baddour-Hadjean, A. Marzouk, J. P. Pereira-Ramos, *J. Raman Spectrosc.* **2012**, *43*–153–160.
[25] R. Baddour-Hadjean, J. P. Pereira-Ramos, C. Navone, M. Smirnov, *Chem. Mater.* **2008**, *20*,–916–1923.
[26] S. H. Lee, H. M. Cheong, M. J. Seong, P. Liu, C. E. Tracy, A. Mascarenhas, J. R. Pitts, S. K. Deb, *Solid State Ionics* **2003**, *165*–111–116.
[27] L. Abello, E. Husson, Y. Repelin, G. Lucazeau, *Spectrochim. Acta Part A Mol. Spectrosc.* **1983**, *39*–641–651.
[28] I. E. Wachs, J. M. Jehng, F. D. Hardcastle, *Solid State Ionics* **1989**, *32–33*–904–910, DOI: 10.1016/0167-2738(89)90374-3.
[29] "Raman spectroscopy-based measurements of thin film thickness | –ACT - Advanced Cooling Technologies," can be found under http://www.1-act.com/case-studies/raman-spectroscopy-based-measurements-of-thin-film-thickness/, **n.d**.
[30] "An Introduction to Electroplating in Engineering and Manufacturing," can be found under http://www.satplating.com/education/an-introduction-to-electroplating/, **n.d**.
[31] R. A. Koochaksaraie, F. Barazandeh, M. Akbari, *Phys. Scr. 98*, 115026.

[32] J. Galy, *J. Solid State Chem.* **1992**, *100*, 229–245.
[33] Y. Liu, M. Clark, Q. Zhang, D. Yu, D. Liu, J. Liu, G. Cao, *Adv. Energy Mater.* **2011**, *1*, 194–202.
[34] X.-F. Zhang, K.-X. Wang, X. Wei, J.-S. Chen, *Chem. Mater.* **2011**, *23*, 5290–5292.
[35] D. Li, Q. Lv, C. Zhang, W. Zhou, H. Guo, S. Jiang, Z. Li, *Batteries.* **2022**, *8*, 101.
[36] L. Bläubaum, F. Röder, C. Nowak, H. S. Chan, A. Kwade, U. Krewer, *ChemElectroChem* **2020**, *7*, 4755–4766.
[37] A. S. M. Sayem Rahman, M. A. Islam, K. M. Shorowordi, *Procedia Eng.* **2015**, *105*, 679–685.
[38] C. S. Yaw, A. K. Soh, M. N. Chong, *MATEC Web Conf.* **2016**, *60*, 01001.
[39] J. H. Yao, Z. L. Yin, Z. G. Zou, Y. W. Li, *RSC Adv.* **2017**, *7*, 32327–32335.
[40] S. Praneetha, Y. S. Lee, V. Aravindan, *J. Ind. Eng. Chem.* **2022**, *112*, 389–397.
[41] Y. L. Cheah, V. Aravindan, S. Madhavi, *ACS Appl. Mater. Interfaces* **2013**, *5*, 3475–3480.
[42] G. Kaur, B. D. Gates, *J. Electrochem. Soc.* **2022**, *169*, 043504.
[43] Y.-S. Hu, X. Liu, J.-O. Müller, R. Schlögl, J. Maier, D. Sheng Su, Y. Hu, J. Maier, X. Liu, J. Müller, R. Schlögl, D. S. Su, *Angew. Chem. Int. Ed.* **2009**, *48*, 210–214.
[44] D. T. Rogstad, M.-A. Einarsrud, A. M. Svensson, *J. Electrochem. Soc.* **2021**, *168*, 110506.
[45] K. Liu, Z. Wang, L. Shi, S. Jungsuttiwong, S. Yuan, *J. Energy Chem.* **2021**, *59*, 320–333.
[46] N.-W. Li, Y.-X. Yin, J.-Y. Li, C.-H. Zhang, Y.-G. Guo, N.-W. Li, Y.-X. Yin, J.-Y. Li, C.-H. Zhang, Y.-G. Guo, *Adv. Sci.* **2017**, *4*, 1600400.
[47] B. Zhao, M. Nisula, A. Dhara, L. Henderick, F. Mattelaer, J. Dendooven, C. Detavernier, B. Zhao, M. Nisula, A. Dhara, L. Henderick, F. Mattelaer, J. Dendooven, C. Detavernier, *Adv. Mater. Interfaces* **2020**, *7*, 2001022.
[48] L. Hongliang, W. Kaiyuan, Y. Zi, Z. Quanchao, C. Yanhua, *Chem. Phys.* **2021**, *544*, 111111.
[49] S. J. Dillon, K. Sun, *Curr. Opin. Solid State Mater. Sci.* **2012**, *16*, 153–162.
[50] E. Peled, S. Menkin, *J. Electrochem. Soc.* **2017**, *164*, A1703–A1719.
[51] V. Jabbari, V. Yurkiv, M. G. Rasul, M. T. Saray, R. Rojaee, F. Mashayek, R. Shahbazian-Yassar, *Energy Storage Mater.* **2022**, *46*, 352–365.
[52] E. E. Ushakova, A. Frolov, A. A. Reveguk, D. Y. Usachov, D. M. Itkis, L. V. Yashina, *Appl. Surf. Sci.* **2022**, *589*, 153014.
[53] E. Armstrong, D. McNulty, H. Geaney, C. O'Dwyer, *ACS Appl. Mater. Interfaces* **2015**, *7*, 27006–27015.
[54] R. L. Puurunen, *J. Appl. Phys.* **2005**, *97*, DOI: https://doi.org/10.1063/1.1940727.
[55] P. Boryło, K. Lukaszkowicz, M. Szindler, J. Kubacki, K. Balin, M. Basiaga, J. Szewczenko, *Vacuum* **2016**, *131*, 319–326.
[56] S. Kim, S. H. Lee, I. H. Jo, J. Seo, Y. E. Yoo, J. H. Kim, *Sci. Reports* **2022**, *12*, 1–6.
[57] M. J. Young, C. B. Musgrave, S. M. George, *ACS Appl. Mater. Interfaces* **2015**, *7*, 12030–12037.
[58] A. W. Ott, J. W. Klaus, J. M. Johnson, S. M. George, *Thin Solid Films* **1997**, *292*, 135–144.
[59] V. Naumann, M. Otto, R. B. Wehrspohn, M. Werner, C. Hagendorf, *Energy Procedia* **2012**, *27*, 312–318.
[60] L. Chen, R. E. Warburton, K. S. Chen, J. A. Libera, C. Johnson, Z. Yang, M. C. Hersam, J. P. Greeley, J. W. Elam, *Chem* **2018**, *4*, 2418–2435.

Manuscript received: October 3, 2023
Revised manuscript received: October 27, 2023
Accepted manuscript online: October 31, 2023
Version of record online: November 22, 2023